Numerical simulation of wave breaking in turbulent two-phase Couette flow

By D. Kim, A. Mani AND P. Moin

1. Motivation and objectives

When a ship moves in the ocean, it generates a surface wave around the ship body. This body-induced wave interacts with turbulent boundary layers in air and water phases, that induces wave breaking, air entrapment and bubble generation. The bubbles can be typically observed by a narrow foam region next to the ship wall and their sizes are from the order of 10 microns to a centimeter for a usual naval surface ship. Especially, the micron-size bubbles reside for a long time beneath the surface because of their low buoyant force and leave a pronounced tail behind the ships. However, it is challenging to understand the bubble formation mechanism and to predict the size distribution of bubbles.

Different mechanisms are involved in the generation of bubbles. The large air cavity or bubbles are entrapped by the plunging wave and they breaks into smaller bubbles by turbulent flows. However, this turbulent fragmentation does not occur to the bubbles whose sizes are smaller than Hinze scale (Deane & Stokes 2002) because the surface tension force prohibits the breakup of the interface. The mechanisms that contribute to generation of sub-Hinze scale bubbles (micro-size bubbles) are the rupture of air films by liquid-liquid or liquid-solid impact (Deane & Stokes 2002; Thoroddsen *et al.* 2010). For example, hundreds of micro bubbles are generated from a single liquid drop impact on the free surface. However, a detailed breakup mechanism of the air film has not been understood yet (Sigler & Mesler 1990; Oguz & Prosperetti 1989; Pumphrey & Elmore 1990).

The objective of the study is to understand the detailed mechanisms of surface breaking, air entrapment, and bubble generation due to interactions between boundary-layers (BL) and free-surfaces (FS) in regimes relevant to naval surface ships. However it is very expensive to simulate the turbulent flow around a ship using direct numerical simulation. Therefore, we propose to investigate turbulent two-phase couette boundary layer flow as a canonical problem through which we can isolate the key phenomena and systematically examine different effects.

In this study, two-phase turbulent boundary layers (TBL) in a Couette-type setting have been simulated, capturing the unsteady evolution of complex phase interface under high liquid-air density-ratio and with surface tension force present at the interface. Computations were carried out for water and air with the Reynolds number of 13,000 and Weber numbers of 42,000 based on the water properties. The primary objective of these calculations is to explore the onset conditions for the breaking of TBL-induced surface waves. Two different Froude numbers, 3.9 and 6.8, are explored to investigate the effect of Froude numbers on the onset of transition to the wave breaking and turbulence statistics.

2. Level set method

2.1. *Governing equations*

The Navier-Stokes equations for incompressible, immiscible, two-phase flow are described as

$$\frac{\partial \rho \mathbf{u}}{\partial t} + \nabla \cdot \rho \mathbf{u}\mathbf{u} = -\nabla \mathbf{p} + \nabla \cdot \tau + \mathbf{T}_\sigma \tag{2.1}$$

$$\nabla \cdot \mathbf{u} = \mathbf{0}, \tag{2.2}$$

where ρ is the density, p the pressure, τ the viscous stress tensor, and $\mathbf{T}_\sigma$ is the surface tension force.

A level set method is applied to track the location of the phase interface. The location and time evolution of the phase interface are described by the level set equation:

$$\frac{\partial G}{\partial t} + \mathbf{u} \cdot \nabla G = 0, \tag{2.3}$$

where the iso-surface $G = 0$ defines the location of the interface, $G > 0$ in the liquid, and $G < 0$ in the gas phase. In the computational domain, G is set to be a signed distance function to the interface:

$$|\nabla G| = 1. \tag{2.4}$$

The interface normal vector $\mathbf{n}$ and the interface curvature κ can be calculated as

$$\mathbf{n} = \frac{\nabla G}{|\nabla G|}, \tag{2.5}$$

$$\kappa = \nabla \cdot \mathbf{n}. \tag{2.6}$$

In this paper, we used the RLSG (Refined Level Set Grid) method (Herrmann 2008) to solve the coupled level set equations (Eqs. 2.3 and 2.4). The level set transport Eq. (2.3) is solved on a separate refined G-grid using a fifth-order WENO scheme (Jiang & Peng 2000) with a third-order TVD Runge-Kutta time discretization (Shu & Osher 1989). It is coupled to the flow solver through $\mathbf{u}$. The velocity $\mathbf{u}$ on the fine G-grid is obtained by trilinear interpolation from the flow solver grid. Reinitialization (2.4) is solved by an iterative procedure using a fifth-order WENO scheme and a first-order pseudo-time integration (Sussman *et al.* 1994; Peng *et al.* 1999). The numerical details about the RLSG method are described in Herrmann (2008).

In order to solve the flow field, the structured grid solver (Pierce & Moin 2011) is used based on a conservative formulation of the variable density Navier-Stokes equations (Kim & Moin 2001). The Navier-Stokes equations are coupled to the level set equation through the density, viscosity and surface tension force. The density ρ and the viscosity μ in a cell i are defined as volume averaged quantities:

$$\rho_i = \psi_i \rho_l + (1 - \psi_i)\rho_g \tag{2.7}$$

$$\mu_i = \psi_i \mu_l + (1 - \psi_i)\mu_g, \tag{2.8}$$

where the subscript l denotes quantities in the liquid and the subscript g denotes those in the gas phase. The flow solver volume fraction ψ is defined as

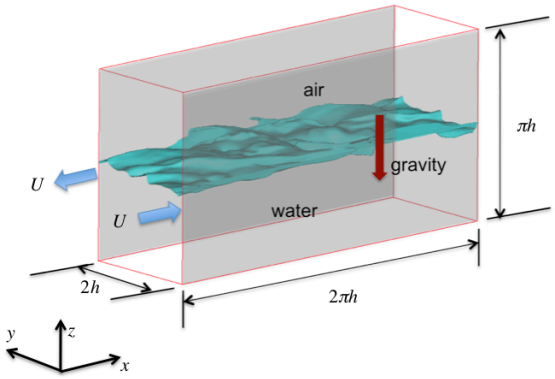

FIGURE 1. Computational domain of two-phase Couette flow with air/water interface.

$$\psi_i = \frac{1}{V_i}\int_{V_i} H(G)dV, \tag{2.9}$$

where H is the Heaviside function and V_i is the control volume of the flow solver grid cell. In the RLSG method, this integral is calculated on the G-grid as

$$\frac{1}{V_i}\int_{V_i} H(G)dV = \frac{\sum_{i_G}\psi_{i_G}V_{i,i_G}}{\sum_{i_G}V_{i,i_G}}, \tag{2.10}$$

where V_{i,i_G} is the joined intersection volume of the G-grid cell i_G and the flow solver control volume V_i, and the G-grid volume fraction ψ_{i_G} is calculated using an analytical formula developed by van der Pijl *et al.* (2005),

$$\psi_{i_G} = f(G_{i_G}, \mathbf{n}_{i_G}). \tag{2.11}$$

The surface tension force $\mathbf{T}_\sigma$ is calculated as

$$\mathbf{T}_{\sigma,i} = \int_{V_i}\sigma\kappa\nabla\psi d\mathbf{x}, \tag{2.12}$$

where σ is the surface tension force coefficient. The curvature κ is transferred from the G-grid to the flow solver grid,

$$\kappa = \frac{\sum_{i_G}V_{i,i_G}\delta_{i_G}\kappa_{i_G}}{\sum_{i_G}V_{i,i_G}\delta_{i_G}}, \tag{2.13}$$

where $\delta_{i_G} = 0$ if $\psi_{i_G} = 0$ or $\psi_{i_G} = 1$, and $\delta_{i_G} = 1$ otherwise. The details about the balanced force algorithm and curvature are described in Herrmann (2008).

3. Numerical simulation of turbulent two-phase Couette flow

3.1. *Numerical configuration*

The flow configuration and domain size are described in Figure 1. The initial shape of the interface is a flat surface in xy plane at the midpoint of $z-$axis. The sidewalls are

moving in the opposite direction with speed of U. The velocity conditions at the top and bottom walls are

$$w = 0, \quad \frac{\partial u}{\partial z} = \frac{\partial v}{\partial z} = 0. \tag{3.1}$$

The flow is assumed to be statistically homogeneous in x-direction where periodic boundary conditions are used. The grid resolution is determined based on the viscous length in the turbulent water flow. The uniform grid spacing, $\Delta x^+ = 20$ and $\Delta z^+ = 15$ in wall units, are used in x and z directions, respectively. In y-direction, strong flow gradients are expected near the wall so that non-uniform grid spacing is applied with fine grid spacing near the sidewalls. A hyperbolic tangent function is employed for the stretching function with $\Delta y^+_{min} = 0.2$ and $\Delta y^+_{max} = 15$. The number of computational cells is $N_x \times N_y \times N_z$=176 × 166 × 176. Computations were carried out for water and air with $\rho_a/\rho_w = 0.0012$ and μ_a/μ_w=0.02, where a and w denote air and water phases. The Reynolds and Weber numbers based on the water properties are $Re_w = \rho_w U h/\mu_w = 12,760$ and $We_w = \rho_w U^2 h/\sigma = 41,600$, respectively. For air flow, the Reynolds and Weber numbers are set to $Re_a = 855$ and $We_a = 50$, respectively. The water and air flows are both turbulent, and turbulent Reynolds numbers are then $Re^w_\tau = 660$ and $Re^a_\tau = 150$ in water and air phase, respectively. The effect of Froude numbers on the characteristics of surface wave was examined for two different Froude numbers of $Fr = U/\sqrt{gh}$=3.9 and 6.8.

3.2. *Results*

Figure 2 shows a snapshot of the phase interface for two different Froude numbers. For the low Froude number case of $Fr = 3.9$, the oblique wave structure is observed and the phase interface is found to be oscillating. However, the breakup into air bubbles hardly occurs at $Fr = 3.9$. On the other hand, the amplitude of surface wave is increased in the case of the high Froude number, $Fr = 6.8$, leading to breakup of the phase interface. The air cavities are found underneath the free surface, which was trapped between the breaking free surface waves. Thus, lots of air bubbles are fragmented by turbulence from the air cavities at $Fr = 6.8$. The characteristics of surface wave for the different Froude numbers is represented in Figure 3, which depicts the mean and rms values of volume fraction in z-direction at $y/h = 1.0$. Note that the volume fraction is 1 in the water phase and 0 in the air phase and the mean Volume fraction is obtained averaged only in the periodic direction (x axis). From the area of VoF_{rms} in Figure 3, the average amplitude of oscillation on the surface wave can be calculated as.

$$A_m = \frac{1}{0.25} \int VoF_{rms} dz. \tag{3.2}$$

We have obtained $A_m = 1.18h$ for $Fr = 6.8$ while $A_m = 0.46h$ for $Fr = 3.9$, which clearly shows the amplitude is proportional to the Froude number.

Figure 4 shows the air ligament formation and air-bubble fragmentation in the case of $Fr = 6.8$. Turbulent water flow contains eddies in various sizes and these eddies lead to ligament formation from the interfacial corrugations. When the size of bubble is larger than the Hinze scale, the bubble is fragmented into ever smaller bubbles by turbulence. However, the turbulent fragmentation ceases at the scale smaller than the Hinze scale where the surface surface tension is large enough to prevent the interfacial breakup. Per unit volume, the kinetic energy of turbulent eddy in water flow is scaled as

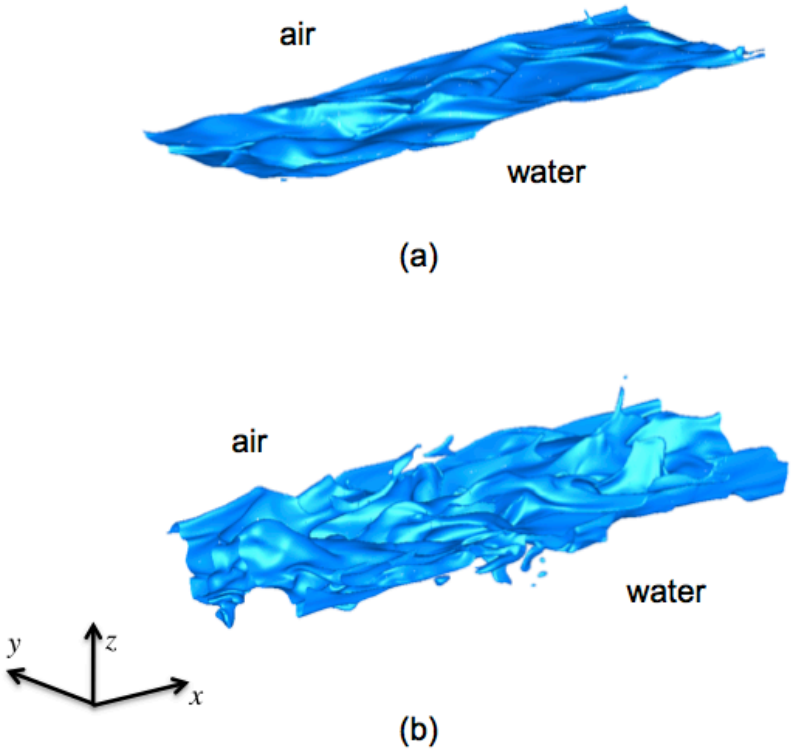

FIGURE 2. Snapshots of air-water interface: (a) $Fr = 3.9$; (b) $Fr = 6.8$.

$$E_k \sim \rho_w v_{l_m}'^2, \tag{3.3}$$

where v_{l_m}' is the turbulent velocity related with the turbulent eddy with size of l_m. The energy associated with surface tension is then scaled as

$$E_s \sim \sigma / l_m, \tag{3.4}$$

where σ is the surface tension coefficient. If E_k is larger than E_s, then the interface is expected to deform and the ligament starts to form. In the inertial subrange, we can use the Kolmogorov hypothesis:

$$\frac{v_l'^3}{l} \sim \frac{v_{l_m}'^3}{l_m} \sim \frac{v'^3}{\eta} \sim \epsilon, \tag{3.5}$$

where l is the size of the largest turbulent eddies, v_l' is the corresponding velocity, η is the Kolmogorov length scale. In the present analysis, l is set to h, and v_l' is set to U. Since E_k can be expressed as $\rho_w \epsilon^{2/3} l_m^{2/3}$ from Eqs. 3.3 and 3.5, E_k decreases for smaller values of l_m, whereas E_s increases. Thus, we can estimate the smallest length scale ξ in the interfacial perturbation where $E_k \sim E_s$. The relation of the smallest length scale to the Weber number is then estimated by

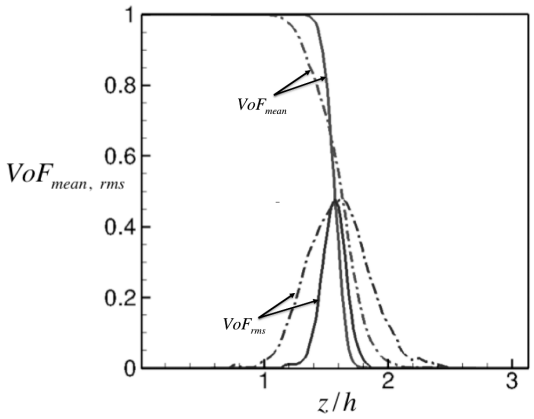

FIGURE 3. Mean and rms values of water volume fraction at for two different Froude numbers: ——, $Fr = 3.9$; – · – ·–, $Fr = 6.8$.

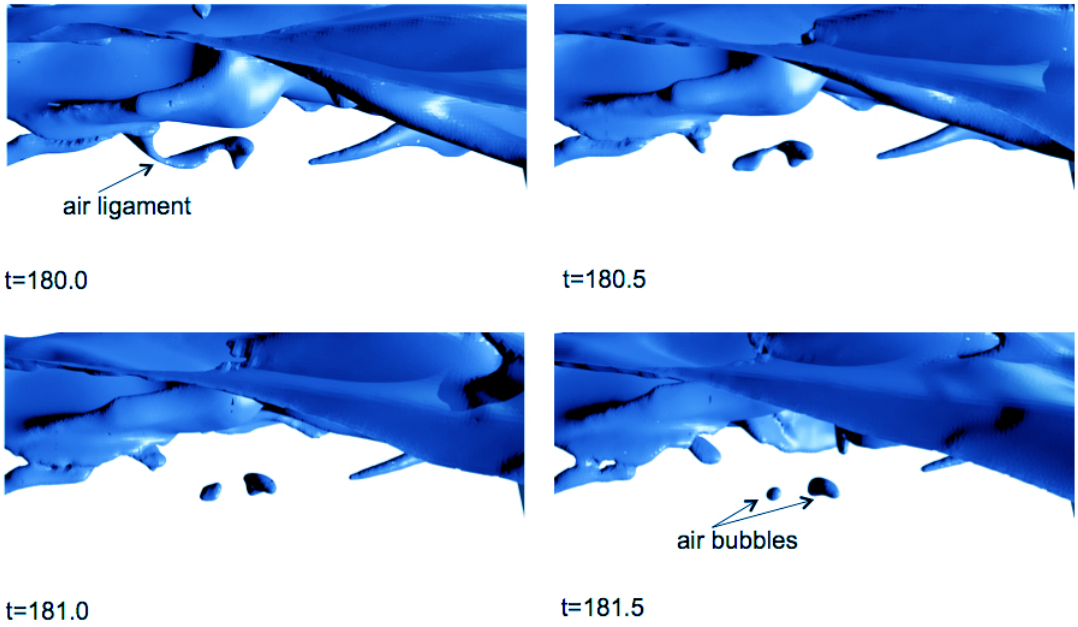

FIGURE 4. Air ligament formation and breakup into bubbles at $Fr = 6.8$.

$$\frac{\xi}{h} \sim \left(\frac{\sigma}{\rho_w v_h^2 h}\right)^{3/5} = We_w^{-3/5}. \tag{3.6}$$

Thus, the small ligament structures are strongly influenced by the Weber number, which can affect the air entrapment and small-size bubble generation.

In order to show the turbulence statistics near the moving sidewall, the mean streamwise velocity profiles and velocity fluctuations in water flow are depicted at $z/h = \pi/4$ along y-direction in Figures 5 and 6, respectively. The turbulence statistics near the mov-

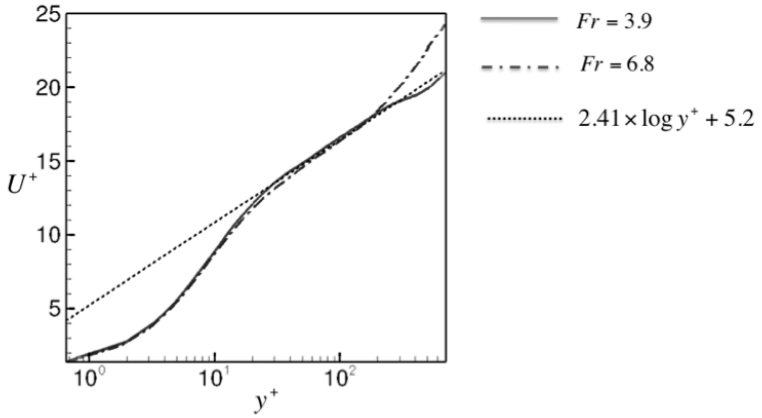

FIGURE 5. Mean streamwise velocity profiles at for two different Froude numbers with log law.

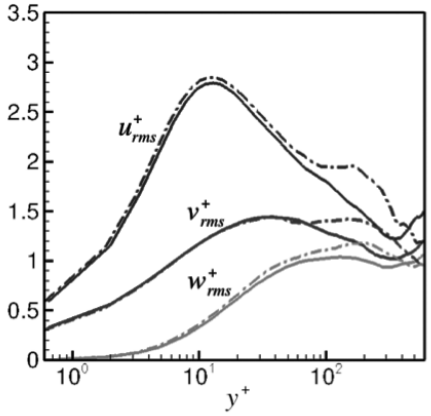

FIGURE 6. Turbulence fluctuations for two different Froude numbers: ——, $Fr = 3.9$; – · – · –, $Fr = 6.8$.

ing walls are similar with that of channel. It is also observed that the Froude number does not affect the turbulence statistics very near the wall.

4. Conclusion

In this study, we present results from two-phase TBLs in a Couette-type setting, capturing the unsteady evolution of the complex phase interface under a high liquid-air density-ratio and with surface tension force present at the interface. Computations were carried out for water and air with the Reynolds number of 13,000 and Weber numbers of 42,000 based on the water properties. Our simulations successfully predict both breaking and non-breaking surface wave regimes at Froude numbers 6.8 and 3.9 respectively. Our results confirm strong dependence of breaking on the Froude number. The air cavity is trapped between the oblique breaking waves only for high Froude number. Thus, air bubbles at various scales are generated from the air cavity at $Fr = 6.8.$, while no air

cavity is found at $Fr = 3.9$. Dependence of turbulence statistics on the Froude number is explored indicating most Froude sensitivity in the outer region of boundary layers.

In the future study, we would like to explore dependence on other parameters. Realistic two-phase boundary layers relevant to naval surface ships are at significantly higher Reynolds numbers than what has been explored here. Therefore, it is necessary to extend our calculations to regimes with higher Reynolds numbers. Furthermore, numerical simulations with finer grid resolution will be done for the grid-independence study, as well as the Lagrangian bubble tracking method with subgrid breakup model for the analysis of bubble size distribution.

Acknowledgments

Authors thank Marcus Herrmann and Frank Ham for discussions and helpful advices. The work presented in this paper was supported by the Office of Naval Research.

REFERENCES

Deane, G. B. & Stokes, M. D. 2002 Scale dependence of bubble creation mechanisms in breaking waves. *Nature* **418** (6900), 839–844.

Herrmann, M. 2008 A balanced force refined level set grid method for two-phase flows on unstructured flow solver grids. *J. Comput. Phys.* **227**, 2674–2706.

Jiang, G. & Peng, D. 2000 Weighted eno schemes for hamilton-jacobi equations. *SIAM Journal on Scientific Computing* **21**, 2126–2143.

Kim, D. & Moin, P. 2001 Progress variable approach for large-eddy simulation of turbulent combustions. *Report No. TF-80, 2001, Stanford University* .

Oguz, H. N. & Prosperetti, A. 1989 Surface-tension effects in the contact of liquid surfaces. *J Fluid Mech* .

Peng, D., Merriman, B., Osher, S., Zhao, H. & Kang, M. 1999 A pde-based fast local level set method. *Journal of Computational Physics* **155** (2), 410 – 438.

Pierce, C. & Moin, P. 2011 Direct numerical simulation of two-phase flows with application to air layer drag reduction. *Report No. TF-125, 2001, Stanford University* .

Pumphrey, H. C. & Elmore, P. A. 1990 Entrainment of bubbles by drop impacts. *Journal of Fluid Mechanics* .

Shu, C. & Osher, S. 1989 Efficient implementation of essentially non-oscillatory shock-capturing schemes, ii. *Journal of Computational Physics* **83** (1), 32–78.

Sigler, J. & Mesler, R. 1990 The behavior of the gas film formed upon drop impact with a liquid surface. *Journal of Colloid and Interface Science* **134** (2), 459–474.

Sussman, M., Smereka, P. & Osher, S. 1994 A level set approach for computing solutions to incompressible two-phase flow. *Journal of Computational Physics* **114** (1), 146 – 159.

Thoroddsen, S. T., Takehara, K. & Etoh, T. G. 2010 Bubble entrapment through topological change. *Physics of Fluids* **22** (5), 051701.